The Bioscan AN INTERNATIONAL QUARTERLY JOURNAL OF LIFE SCIENCES 20(2): S2: 565-575, 2025 www.thebioscan.com

Synthesis, Characterisation, Biological Evaluation, and Computational Studies of a Novel Tetraaza Amide Macrocyclic Ligand and Its Metal Complexes Targeting Glioblastoma and HDAC II Inhibition

P. YOGALAKSHMI[1], N. BANUMATHI[2]

1. Research scholar (Chemistry), Rani Anna Government College for Women, Affiliated to Manonmaniam Sundaranar University, Tirunelveli- 627 008, Tamilnadu, India

Email: s.dharu1996@yahoo.com

2. Assistant Professor, Department of Chemistry, Chikkanna Government Arts College, Affiliated to Bharathiar University, Tirupur,641602, Tamil Nadu, India

Email: mobapra33@yahoo.co.in

DOI: 10.63001/tbs.2025.v20.i02.S2.pp565-575

KEYWORDS
Tetraaza macrocycle, HDAC II inhibition, Glioblastoma, Cytotoxicity, Molecular docking

Received on:

08-04-2025

Accepted on:

05-05-2025

Published on:

02-06-2025

ABSTRACT

This study reports the synthesis and comprehensive evaluation of a novel tetraaza amide macrocyclic ligand and its Co(II), Ni(II) and Zn(II) complexes, aimed at targeting glioblastoma multiforme (GBM) and inhibiting human Histone Deacetylase II (HDAC II). The compounds exhibited significant antimicrobial, antioxidant, and anticancer activities, with notable cytotoxicity against U87 glioma cells confirmed via MTT assay and apoptosis induction. In silico profiling using SwissADME and admetSAR presented conflicting drug-likeness results but indicated favorable blood-brain barrier permeability and low toxicity. Quantum chemical analyses and molecular docking revealed strong binding affinities to HDAC-II, supporting their potential as therapeutic agents for GBM. Overall, the findings suggest that the metal complex 2phapZn represents a promising multi-targeted candidate for glioma treatment and epigenetic therapy, with additional antimicrobial and antioxidant benefits.

INTRODUCTION

Macrocyclic ligands have emerged as pivotal candidates in the realm of medicinal chemistry, owing to their exceptional structural attributes, intrinsic stability, and significant biological activities [1]. Among these, tetra aza amide macrocyclic ligands, characterized by four nitrogen donor atoms and strategically positioned amide functionalities, have gained widespread attention for their broad applicability in bioinorganic chemistry and pharmaceutical development. These macrocycles are adept at forming robust complexes with transition metals, enabling fine-tuning of their chemical, biological, and pharmacokinetic properties.

The present investigation focuses on the synthesis, characterization, and extensive biological evaluation of a novel tetraaza amide macrocyclic ligand and its metal complexes, aimed at combating brain glioma (U87 cell line) and inhibiting human Histone Deacetylase II (HDAC II) enzymes. Brain glioma, notably derived from U87 cells, remain among the most aggressive and therapeutically challenging tumors, characterized by rapid proliferation, resistance to conventional therapies, and poor prognosis. There is a compelling need for novel therapeutic agents capable of overcoming these barriers [3].

Macrocyclic complexes, with their unique capability to penetrate biological membranes, interact with nucleic acids, and modulate enzymatic activities, offer promising alternatives for glioma treatment [4]. Simultaneously, histone deacetylases, particularly HDAC II, play crucial roles in regulating gene expression by modifying chromatin architecture [5]. Aberrant HDAC activity is linked to tumorigenesis, making HDAC inhibitors attractive targets for anticancer drug development [6]. In addition to their anticancer potential, the antimicrobial properties of macrocyclic compounds have been well documented. Their mechanisms typically involve membrane disruption, interference with enzymatic systems, and induction of oxidative stress within microbial cells [7].

Evaluating the antibacterial and antifungal activities of the synthesized ligand and its complexes is crucial for understanding their therapeutic potential [8]. The need for dual-acting agents, particularly relevant for immunocompromised patients, is also

addressed in this context [9]. Furthermore, the antioxidant capacity of the novel compounds can be explored through radical scavenging assays [10], given the established correlation between oxidative stress, cancer progression, and inflammatory disorders [11]. Cytotoxic evaluations against the U87 glioma cell line were conducted via MTT assays to determine cell viability post-treatment [12]. Additionally, apoptosis, a form of programmed cell death, was confirmed through staining techniques such as acridine orange/ethidium bromide staining [13].

Pharmacokinetic predictions were performed using SwissADME and admetSAR platforms to assess drug-likeness, solubility, absorption, distribution, metabolism, excretion, and toxicity (ADMET) profiles[14]. These in silico analyses are crucial for forecasting the compounds' success in biological systems and minimizing potential toxicities. Quantum chemical calculations, including HOMO-LUMO energy gaps, were undertaken to investigate the electronic behavior of the compounds [15]. The energy gap between the frontier molecular orbitals offers insights into the chemical reactivity, kinetic stability, and potential interaction mechanisms with biological targets [16]. Additionally, global chemical descriptors such as hardness, softness, electronegativity, electrophilicity, and nucleophilicity were computed to further elucidate the reactivity patterns and stability of the synthesized entities [17]. These descriptors are predictive of how the compounds might behave under physiological conditions. Molecular Electrostatic Potential (MEP) mapping was utilized to visualize charge distributions within the molecules, thereby identifying regions susceptible to electrophilic or nucleophilic attacks [18]

Molecular docking studies were conducted to predict and model the interaction between the synthesized compounds and the HDAC II enzyme [19]. Docking results offer valuable information regarding binding affinities, modes of interaction, and potential inhibitory mechanisms, reinforcing the experimental findings and highlighting the therapeutic relevance of the compounds. In conclusion, this comprehensive study integrates synthetic, biological, computational, and pharmacokinetic evaluations to assess the therapeutic promise of a novel tetraaza amide macrocyclic ligand and its metal complexes [20]. By simultaneously targeting brain glioma cells and HDAC II enzymes, and demonstrating antimicrobial, antioxidant, and cytotoxic potentials, the findings contribute to the advancement of novel multi-target chemotherapeutic agents with enhanced efficacy and favorable pharmacological profiles suitable for future clinical development.

II. METHODOLOGY

All reagents and solvents were of analytical grade and used as received. Diethyl oxalate, o-phenylenediamine, and metal salts ($CoCl_2 \cdot 6H_2O$, $NiCl_2 \cdot 6H_2O$, $ZnCl_2$) were obtained from E. Merck. Conductivity measurements were carried out in dry DMF using a Model 601 conductivity bridge. Melting points were determined using an electric melting point apparatus. UV-visible diffuse reflectance spectra were recorded at room temperature with a Jasco V750 spectrophotometer, while FT-IR spectra were obtained using a Shimadzu IR Affinity-I spectrophotometer.

2.1. Synthesis of tetraaza macrocyclic amide ligand (2phap): (6,11,18,23-Tetraazatetrabenzo[a, c,i,k]cyclohexadecane-5,12,17,24-tetrone), $C_{28}H_{20}N_4O_4$)

The macrocyclic ligand 6,11,18,23-Tetraazatetrabenzo[a,c,i,k]cyclohexadecane-5,12,17,24-tetrone ($C_{28}H_{20}N_4O_4$) was synthesized via a condensation reaction between diethyl phthalate (4 mL, 0.02 mol) and o-phenylenediamine (2.163 g, 0.02 mol) in the presence of concentrated hydrochloric acid (0.02 mol). Refluxing the mixture resulted in a red precipitate, which was subsequently filtered and washed with tetrahydrofuran (THF), diethyl ether, and petroleum ether. Due to the low yield of the ligand, a template synthesis strategy was adopted to prepare its metal complexes. The synthetic pathway for the tetra aza macrocyclic amide ligand is illustrated in Figure 1.

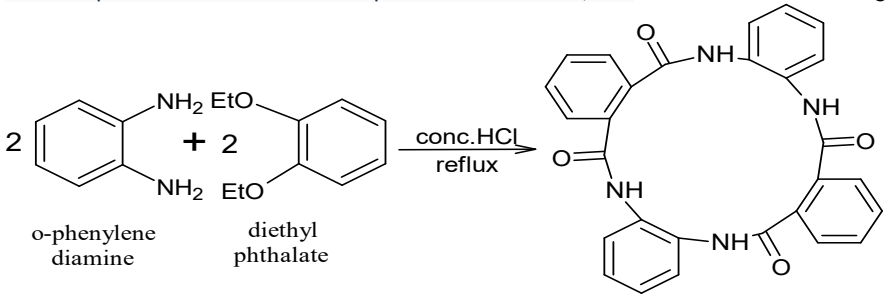

Figure 1. synthesis of 2phap ligand

2.2. Synthesis of Complexes (2phapCo, 2phapNi and 2phapZn): $[Co(C_{28}H_{20}N_4O_4)Cl_2]$, $[Ni(C_{28}H_{20}N_4O_4)]\ Cl_2$ and $[Zn(C_{28}H_{20}N_4O_4)]\ Cl_2$

A hot ethanolic solution of diethyl phthalate (4 mL, 0.02 mol) was combined with a hot solution of o-phenylenediamine (2.163 g, 0.02 mol) and refluxed. Ethanolic solution of the respective metal chloride (0.1mol) (dry $ZnCl_2$, $NiCl_2 \cdot 6H_2O$, or $CoCl_2 \cdot 6H_2O$) was then added gradually under continuous stirring during the reflux process. After one hour of refluxing, a colored precipitate formed, which was subsequently filtered and thoroughly washed with petroleum ether, ethanol, THF, and diethyl ether [21].

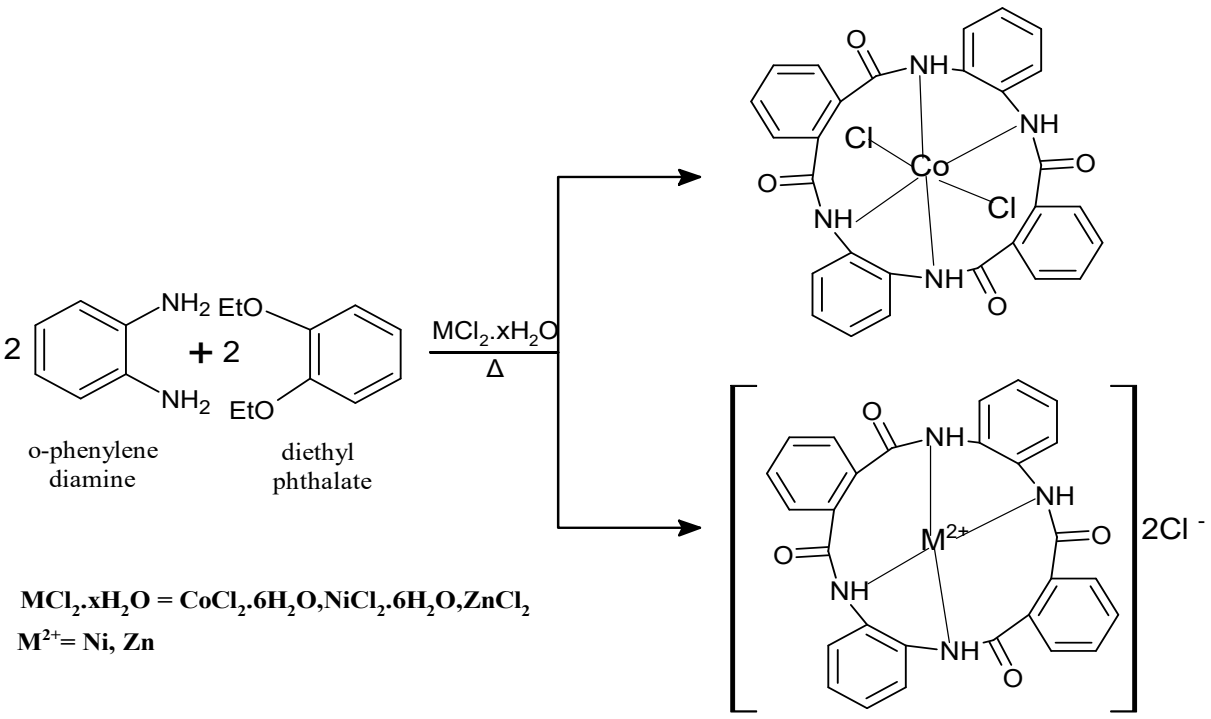

Figure 2 . synthesis of 2phap metal complexes

2.3. Preliminary Test for Water Molecule and Chloride Ion

The presence of water molecules in the crystallized metal complexes was assessed using cobalt chloride paper. The lack of a color change from blue to pink indicated the absence of water within the crystal lattice. To detect uncoordinated chloride ions, those not directly bonded to the metal center aqueous silver nitrate ($AgNO_3$) and ammonium hydroxide (NH_4OH) were added to solutions of the complexes. The immediate formation of a white precipitate, which dissolved upon the addition of excess NH_4OH, confirmed the presence of free chloride ions outside the metal coordination sphere [22].

2.4. ADMET analysis

The pharmacokinetic profiles of the synthesized drug candidates were evaluated using the SwissADME web tool (http://www.swissadme.ch/), which predicts key ADME (absorption, distribution, metabolism, and excretion) parameters. SMILES (Simplified Molecular Input Line Entry System) representations of the compounds were employed to assess their drug-likeness and pharmacokinetic suitability. Additionally, potential toxicity was predicted using the admetSAR platform (https://lmmd.ecust.edu.cn/admetsar2), facilitating a preliminary evaluation of their safety profiles.

2.5. In silico molecular docking studies

2.5.1. Retrieval of the tertiary structure of protein and structure validation

To identify potential protein targets of the synthesized compounds, their SMILES notations derived from 3D molecular structures were submitted to the Therapeutic Target Database (TTD). Target proteins were subsequently validated using the UniProt database, and corresponding Protein Data Bank (PDB) identifiers were retrieved. Specifically, the 3D crystal structure of the HDAC-II enzyme complexed with N-(2-aminophenyl) benzamide (PDB ID: 3MAX) was obtained from the RCSB Protein Data Bank. This structure, provided in PDB format, was energy-minimized using Swiss-PDB Viewer (version 4.1.0) to optimize atomic coordinates and improve structural reliability. Structural validation was performed through a Ramachandran plot generated via the PDBsum server (https://www.ebi.ac.uk/thornton-srv/databases/pdbsum/). Furthermore, the overall quality of the protein model was assessed using the ProSA web tool (https://prosa.services.came.sbg.ac.at/prosa.php), which analyzed the Z-score to confirm its suitability for further computational studies.

2.5.2. Binding pocket prediction

Protein active site prediction was performed using the machine learning Prank web server (https://prankweb.cz/), which identifies potential ligand binding regions within a protein structure. These binding sites are essential for molecular recognition and catalytic function, as they serve as specialized domains that enable interactions with specific substrates or ligands, thereby influencing biological activity.

2.5.3. Ligand designing and preparation

To evaluate their potential interactions with the target enzyme, the synthesized compounds were structurally optimized, converted into PDB format, and then subjected to molecular docking study.

2.5.4 Molecular Docking Analysis

To evaluate the anticancer potential of synthesized compounds targeting the HDAC-II enzyme, molecular docking studies were performed against the approved drug suberoylanilide hydroxamic acid (SAHA) as a benchmark. The HDAC-II receptor structure (chains A, B, C) was retrieved, and chain A was selected for these docking studies. Protein preparation involved removing water molecules and extraneous ions, adding polar hydrogen atoms to account for tautomeric and oxidation state adjustments, and crucially retaining the essential zinc ion for its structural and catalytic role. Flexible ligand docking simulations were then carried out using AutoDock Vina (version 1.5.6). Finally, the resulting ligand protein interactions were analyzed with Biovia Discovery Studio Visualizer, enabling detailed 2D and 3D examination of the binding modes between HDAC-II and both the test and reference compounds.

2.6. DFT Studies

The macrocyclic ligand (2phap) and its Co(II), Ni(II), and Zn(II) complexes were structurally optimized using Density Functional Theory (DFT) without symmetry constraints. These geometry optimizations were performed with Gaussian 16 (Revision C.02) employing the B3LYP functional. The LANL2DZ basis set was applied to the transition metal atoms, while the 6-311++G (d, p) basis set was used for non-metal atoms (C, H, O, N). GaussView 6.0 was used to visualize the optimized geometries. Molecular Electrostatic Potential (MEP) analysis was then conducted to investigate electron density distributions and identify potential reactive sites. Key electronic parameters, including total energy and the energies of the Highest Occupied Molecular Orbital (HOMO) and Lowest Unoccupied Molecular Orbital (LUMO), were also calculated.

2.7. Antimicrobial studies

2.7.1. Antibacterial essay

The antibacterial efficacy of the test compounds (10 mg/mL) was assessed against *Escherichia coli* and *Staphylococcus aureus* using the well diffusion method on nutrient agar. After inoculating the plates, wells were loaded with varying volumes (25–100 µL) of the test solutions. Following incubation at 37°C for 24 hours, antibacterial activity was determined by measuring the zones of inhibition. Chloramphenicol served as the positive control, and all experiments were performed in triplicate.

2.7.2. Antifungal studies

The antifungal activity of the test compounds (10 mg/mL) was evaluated against *Candida albicans* using the well diffusion method on YPD agar. After inoculating agar plates with fungal suspensions, wells were loaded with 25–100 µL of the test solutions. Following incubation under appropriate conditions, antifungal efficacy was determined by measuring the zones of inhibition. Fluconazole served as the positive control, and all assays were performed in triplicate.

2.8. Antioxidant studies

The antioxidant potential of the test samples was evaluated using the DPPH free radical scavenging assay. Various concentrations of the samples (10–50 µg/mL) were mixed with a 0.1 mM DPPH solution and incubated at room temperature for 30 minutes, after which absorbance was measured at 517 nm. L-ascorbic acid (10–500 µg/mL) served as the positive control. Scavenging activity was calculated using the formula: Scavenging effect (%) = $(A_c - A_t)/A_c \times 100$, where A_c is the absorbance of the control and A_t is the absorbance of the test sample

2.9. Cytotoxic studies

In silico analysis using PASS CLC Pred (http://www.way2drug.com/Cell-line/) predicted strong cytotoxic activity for the tetra aza macrocyclic amide ligand against the Uppsala 87 Malignant Glioma (U-87 MG) cell line, highlighting its potential selectivity and therapeutic promise for brain cancer. To experimentally validate this, the cytotoxicity of the tetra aza macrocyclic ligand and its metal complexes was assessed against U-87 MG cells using the MTT assay. Cells were seeded at 50,000 cells/well in 96-well plates and incubated for 24 hours before a 24-hour treatment with various concentrations of the test compounds. Following this, MTT reagent was added and incubated for 4 hours. The resulting formazan crystals were dissolved in DMSO, and absorbance was measured at 570 nm. Percentage growth inhibition was calculated using the formula: % Inhibition = [(OD of control – OD of sample) / OD of control] × 100, where OD of control is the optical density of untreated control cells and OD of sample is that of treated cells. IC_{50} values were then determined by nonlinear regression analysis using GraphPad Prism.

2.10. Apoptosis studies by AO-EB Dual Fluorescent Staining Method

The AO-EB dual staining technique differentiates viable, apoptotic, and necrotic cells through distinct fluorescence and morphology. Acridine Orange (AO) stains all nuclei green, while Ethidium Bromide (EB) selectively enters membrane compromised cells, staining their nuclei orange/red. This approach highlights apoptosis indicators like chromatin condensation and membrane blebbing, thereby facilitating the assessment of drug induced cell death.

III. RESULT AND DISCUSSION

3.1. Characterisation of synthesized compounds

Analytical data (Table 1) confirms the synthesis of the ligand 2phap(2P) from the reaction of diethyl oxalate with o-phenylenediamine. The corresponding macrocyclic Co(II), Ni(II), and Zn(II) complexes 2phapCo(2PC), 2phapNi(2PN), and 2phapZn(2PZ), respectively were synthesized via a template method using a 1:1 molar ratio in ethanolic solution. Both the macrocyclic ligand and its metal complexes are soluble in DMF and DMSO. Key spectral data, including infrared (FT-IR), electronic spectra, and molar conductance measurements, are presented in Table 2

Compound / formula	Mol. weight	Color	M. Point ° C	Yield %	Elemental analysis Calculated (experimental)			
					C	H	N	Cl
2phap (2P) $C_{28}H_{20}N_4O_4$	476.15	pink	150	20	70.58 (69.98)	4.23 (4.22)	11.76 (11.00)	-
[Co(2phap) Cl_2] 2phapCo) (2PC) [Co($C_{28}H_{20}N_4O_4$) Cl_2]	605.02	brown	>250	85	55.47 (55.08)	3.32 (3.18)	9.24 (9.13)	11.69 (11.53)
[Ni(2phap)] Cl_2 (2phapNi) (2PN) [Ni($C_{28}H_{20}N_4O_4$)] Cl_2	606.08	violet	>250	90	55.49 (55.39)	3.33 (3.13)	9.24 (9.12)	11.70 (11.65)
[Zn(2phap)] Cl_2 (2phapZn) (2PZ) [Zn($C_{28}H_{20}N_4O_4$)] Cl_2	610.02	white	180	60	54.88 (54.75)	3.29 (3.23)	9.14 (9.04)	11.57 (11.45)

Table 1. The analytical data and physical properties of 2phap ligand and its metal complexes

In 2phap Ligand, IR Spectroscopy confirms typical amide features: ν(N-H) at 3332 cm^{-1}, ν(C=O) at 1620 cm^{-1}, and Amide III at 1234 cm^{-1}. UV-Vis shows π→π* and n→π* transitions at 204, 238, and 320 nm. DFT reveals secondary amide geometry with C=O and N-H bond lengths of ~1.23 Å and ~1.02 Å, respectively. In the Cobalt complex[23], a distorted octahedral geometry is confirmed by DFT (Co-N ~2.02 Å, Cl-Co-Cl ~83.4°, trans N-Co-N ~149°). IR indicates nitrogen coordination with a ν(N-H) shift to 3356 cm^{-1} and unchanged ν(C=O), ruling out oxygen involvement. New metal-ligand bands at 424 and 378 cm^{-1} are observed. UV-Vis reveals d-d transitions at 491 and 681 nm (ν_3 and ν_1), consistent with high-spin octahedral Co(II). Molar conductance confirms non-electrolytic nature. IR shows ν(N-H) and ν(C=O) downshifts (3286 to 1296 cm^{-1}, suggesting N-coordination and enhanced intramolecular hydrogen bonding in the Nickel complex[24]. DFT indicates a distorted square planar geometry (Ni-N ~2.045 Å; N-Ni-N angles ~88–91° cis, ~173° trans). UV-Vis features d-d transitions at 364 and 580 nm, typical for square planar d^8 Ni(II). Molar conductance confirms a 1:2 electrolyte. IR data reflect strong intramolecular hydrogen bonding in the Zinc complex[25], with ν(N-H) at 3209 cm^{-1} and ν(C=O) at 1604 cm^{-1}. Amide III shifts to 1280 cm^{-1}, and a ν(Zn-N) vibration at 432 cm^{-1} is observed. DFT reveals a distorted tetrahedral structure (Zn-N ~2.079 Å; N-Zn-N ~86–92° cis, ~165° trans). UV-Vis shows blue-shifted ligand transitions (231, 262 nm) and a weak LMCT band at 387 nm. Molar conductance confirms a 1:2 electrolyte.

Compound	$\sqrt{}_{N-H}$ (cm $^{-1}$)	Amide (cm $^{-1}$)				γ_{M-N} (cm $^{-1}$)	γ_{M-Cl} (cm $^{-1}$)	Molar conductivity (S cm^2 mol $^{-1}$)	ʎ (nm)
		I γ(C=O)	II γ(C-N) + δ (N-H)	III δ(N-H)	Ar. C-H out of plane bending				
2phap (2P) $C_{28}H_{20}N_4O_4$	3332	1620	1519	1234	748	-	-	-	204, 238, 320
[2phapCoCl_2] (2PC) [Co($C_{28}H_{20}N_4O_4$) Cl_2]	3356	1620	1527	1242	748	424	378	16	251, 304, 388, 491, 681
[Ni(2phap)] Cl_2 (2phapNi) (2PN) [Ni($C_{28}H_{20}N_4O_4$)] Cl_2	3286	1604	1573	1296	748	439	-	104	259,292, 364,580
[Zn(2phap)] Cl_2 (2phapZn) (2PZ) [Zn($C_{28}H_{20}N_4O_4$)] Cl_2	3209	1604	1573	1280	756	432	-	113	231, 262, 387

Table 2 The IR, electronic spectral data and molar conductance measurements of 2phap ligand and its metal complexes

3.2. In Silico admet studies

The physicochemical, pharmacokinetic, and toxicity (ADMET) profiles of the synthesized compounds (2phap, 2phapCo, 2phapNi, and 2phapZn) were systematically evaluated against the standard HDAC inhibitor SAHA using SwissADME. Compared to SAHA, the synthesized metal complexes exhibited higher molecular weights, increased hydrogen bond acceptors, and comparable TPSA values, but demonstrated poor water solubility and lower bioavailability scores. Regarding drug likeness, 2phap and SAHA fully complied with Lipinski's rule, whereas the metal complexes showed multiple violations. Pharmacokinetic predictions indicated high gastrointestinal absorption for 2phap and SAHA, but not for the metal complexes; notably, none of the tested compounds, including SAHA, were predicted to cross the blood brain barrier. Importantly, all synthesized compounds were predicted to be non-AMES toxic and non-carcinogenic, in contrast to SAHA, which exhibited AMES toxicity. Overall, 2phap emerged as the most promising candidate due to its superior drug-likeness and favorable pharmacokinetic properties, positioning it as a strong alternative to SAHA for further therapeutic exploration.

compound		2phap	2phapCo	2phapNi	2phapZn	SAHA
Physicochemical properties						
MoLWt (g/mol)		476.48	606.32	606.08	612.77	264.32
HBD		4	4	4	4	3
HBA		4	8	8	8	3
TPSA (A °2)		116.40	116.40	116.40	116.40	78.43
Log P $_{o/w}$		2.84	2.97	1.32	1.33	1.92
Water solubility Log S (ESOL)		-5.39 mod. soluble	-7.59 poorly soluble	-7.59 poorly soluble	-7.63 poorly soluble	-2.22 soluble
Bioavailability score		0.55	0.17	0.17	0.17	0.55
PAINS		0 alert	0 alert	0 alert	0 alert	0 alert
Synthetic accessibility		3.18	4.26	4.21	4.57	1.91
Drug likeness rules	Lipinski rule	Yes 0 violation	2 violation	2 violation	2 violation	Yes 0 violation
	Ghose rule	1 violation	2 violation	3 violation	3 violation	Yes 0 violation
	Veber rule	Yes 0 violation	Yes 0 violation	Yes 0 violation	Yes 0 violation	Yes 0 violation
	Egan rule	Yes 0 violation	Yes 0 violation	Yes 0 violation	Yes 0 violation	Yes 0 violation
	Muegge rule	Yes 0 violation	3 violation	3 violation	3 violation	Yes 0 violation
Pharmacokinetic properties and Toxicity						
BBB		no	no	no	no	no
GIA		high	high	low	low	high
P-gp substrate		no	Yes	Yes	Yes	No
Log K_p		-6.84	-6.02	-6.01	-6.05	-6.59
Caco2 permeability		0.5530	0.5495	0.5442	0.5442	0.8957
AMES toxicity		NonAMES	NonAMES	NonAMES	NonAMES	AMES, toxic
Carcinogenicity		Non-carcinogenic	Non-carcinogenic	Non-carcinogenic	Non-carcinogenic	Non-carcinogenic

Table 3. The ADMET properties of the 2phap ligand and its complexes from SWISS ADME and admetSAR server

3.3. In silico molecular docking studies

Molecular docking studies targeting HDAC-II revealed 2phapZn as the most potent binder among the synthesized compounds (2phap, 2phapCo, 2phapNi), with a binding affinity of -8.7 kcal/mol, surpassing the benchmark HDAC inhibitor SAHA (-7.3 kcal/mol). This superior binding is attributed to multiple stabilizing interactions, including hydrogen bonds, van der Waals forces, attractive charges, and π-interactions with key active site residues. These findings suggest 2phapZn could be a more effective HDAC2 inhibitor than SAHA, offering the stronger and more diverse molecular engagements critical for epigenetic modulation. Consequently, 2phapZn's superior docking performance highlights its potential as a promising lead compound for developing novel HDAC II targeted therapeutics, particularly for glioma treatment.

s.no.	compound	Binding energy kcal/ mol	Conventional Hydrogen bond	Vanderwaals interaction	Hydrophobic interactions	Electrostatic interaction	Attractive charge	Pi-Sulphur
1	2phap	-8.1	PHE210	ASP104, HE155, GLY154, HIS183, TYR209	PHE210, LEU276	-	-	-
2	2phapCo	-6.5	PHE210	PHE155, HIS183, GLU208, TYR209, ARG275	LEU276, CYS278	-	-	-
3	2phapNi	-7.4	-	PRO34, PHE155, GLU208, TYR209, PHE210	HIS183, LEU276	HIS183	-	-
4	2phapZn	-8.7	HIS183	HIS146, GLY154, LEU276	PHE155, PHE210	-	Asp104	-
5	SAHA	-7.3	HIS145, HIS183, GLY306, GLY143	LEU276, ASP104, PHE210, PHE114, TYR29	MET35, PHE155, HIS146, PHE155, HIS183, LEU144, ARG39, TYR308, GLY305, Zn379, GLY154, ASP181, GLN265	-	-	CYS156

Table 4. The binding energy and interactions of the 2phap ligand and its metal complexes with the receptor (3MAX):

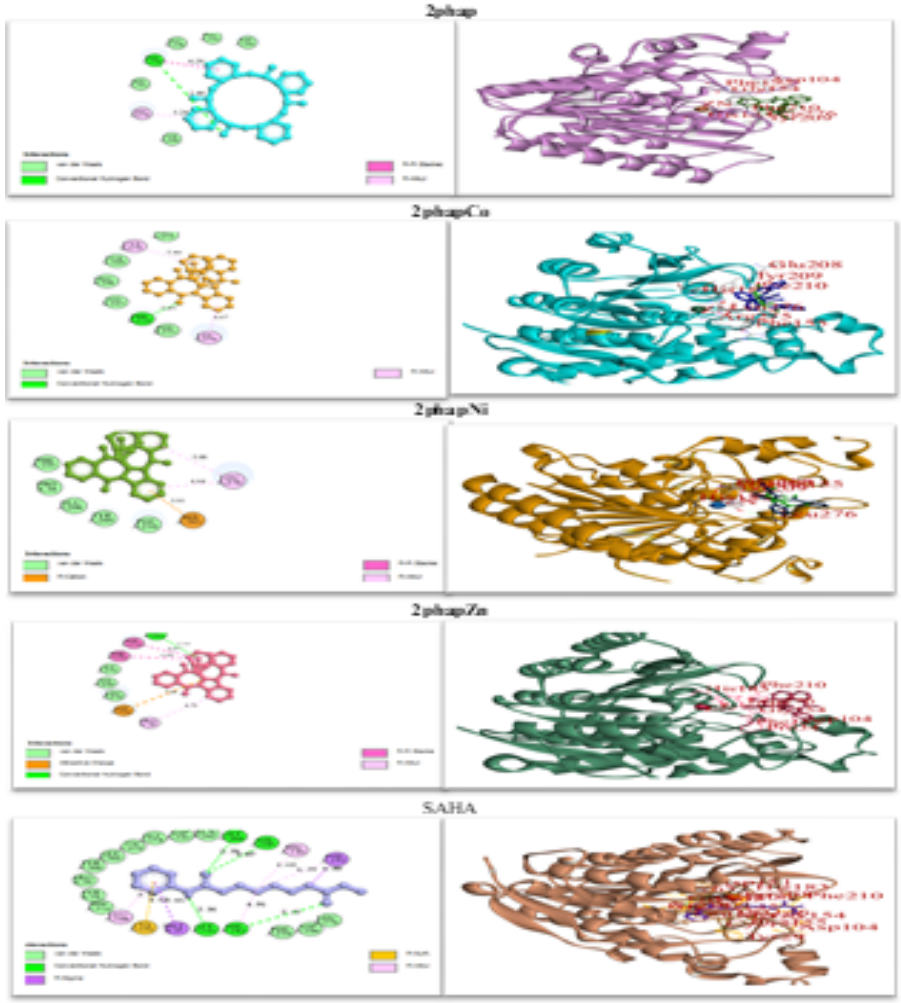

Figure 3. The 2D (left) and 3D (right) docking poses of the 2phap ligand and its complexes with the receptor 3MAX

3.4. DFT studies

Figure 4 displays the optimized structures of the 2phap ligand and its complexes, derived using Gaussian16 (Revision C.02) and visualized with GaussView 6.0. Density Functional Theory (DFT) analysis shown in Table 5 revealed distinct electronic and stability profiles for the synthesized compounds. 2phapCo exhibited the greatest thermodynamic stability (energy: -1773.6496 a.u.), while 2phapNi displayed the highest dipole moment (11.6579 D). Crucially, 2phapZn demonstrated the smallest bandgap (1.1081 eV) shown in Figure 5, highest chemical softness, and strongest electrophilicity (8.3965 eV), indicative of superior chemical reactivity. This contrasted with SAHA, which presented a wider bandgap (5.6472 eV) and greater chemical hardness (2.8236 eV), reflecting higher stability but consequently lower reactivity.

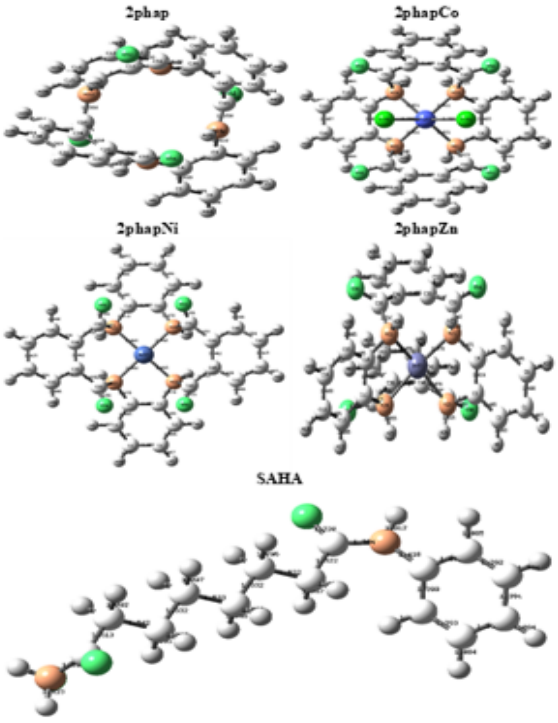

Figure 4 The optimized geometry of the synthesis compound utilizing B3LYP/LANL2D 6-311++G (d,p) level of calculation

Comp	2phap	2phapCo	2phapNi	2phapZn	SAHA
Energy (a.u)	-1599.4395	-1773.6496	-1767.9637	-1664.1890	-880.9455
Dipolemoment (μ)	0.9524	9.5706	11.6579	8.3028	2.5246
E_{HOMO} (Hartree)	-0.20840	-0.24384	-0.11712	-0.13247	-0.24345
E_{LUMO} (Hartree)	-0.09939	-0.06591	-0.07219	-0.09175	-0.03592
E_{HOMO} (eV)	-5.6708	-6.6352	-3.1870	-3.6047	-6.6246
E_{LUMO} (eV)	-2.7045	-1.7935	-1.9644	-2.4966	-0.9774
Bandgap (ΔE)	4.8417	2.9663	1.2226	1.1081	5.6472
IP (eV)	5.6708	6.6352	3.1870	3.6047	6.6246
EA (eV)	2.7045	1.7935	1.9644	2.4966	0.9774
Electro Negativity (χ) eV)	4.2144	4.1877	2.5757	3.0507	3.8010
Chemical potential (μ) (eV)	-4.2144	-4.1877	-2.5757	-3.0507	-3.8010
Chemical hardness (η) (eV)	2.4209	1.4832	0.6113	0.5542	2.8236
Chemical softness (σ) (eV)	0.4131	0.6742	1.6358	1.8044	0.3541
Global softness (S) (eV^{-1})	0.2066	0.3371	0.8179	0.9022	0.1771
Electrophilicity index (ω) (eV)	3.6695	2.0939	5.4261	8.3965	1.4118
nucleophilicity index (N)	0.2725	0.4776	0.1843	0.1191	0.7083

Table 5 The predicted quantum chemical descriptors for 2phap ligand, its complexes and reference compound

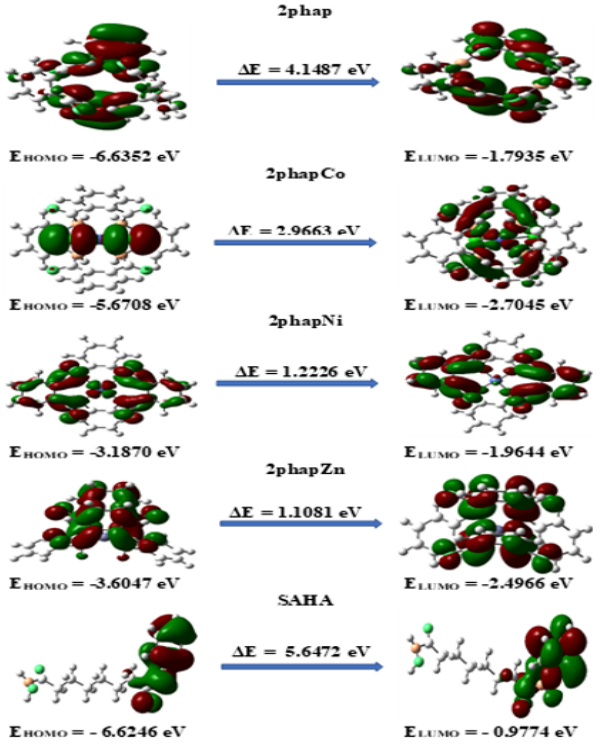

Figure5.The frontier molecular orbitals of the 2phap ligand and its complexes calculated from DFT approach

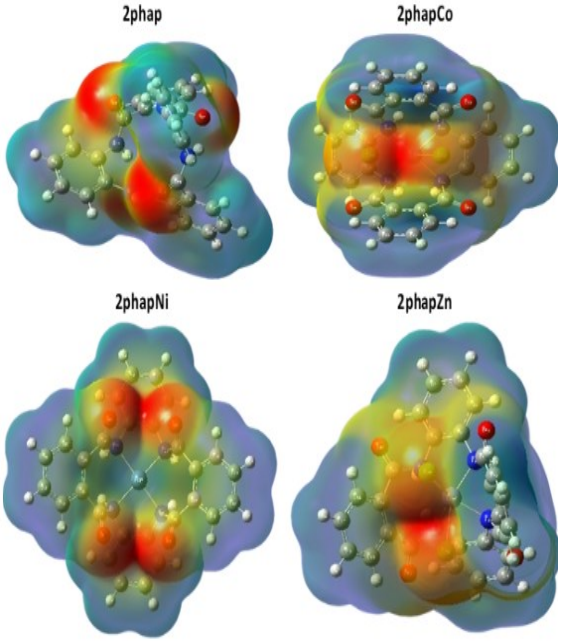

Figure 6. The molecular electrostatic potential of the 2phap ligand and its complexes from DFT approach

These DFT derived electronic properties, particularly the enhanced reactivity of 2phapZn, strongly correlated with its molecular docking performance. Specifically, 2phapZn showed the highest binding affinity towards HDAC II, surpassing SAHA. It is proposed that 2phapZn's high reactivity facilitates stronger and more diverse molecular interactions within the HDAC II active site, thereby enhancing its inhibitory potential. Considering HDAC II's critical role in glioma progression, these integrated findings underscore 2phapZn's significant promise as a potent epigenetic modulator for glioma therapy, potentially offering advantages over the conventional HDAC inhibitor SAHA.

3.5. Molecular electrostatic potential maps

The Molecular Electrostatic Potential (MESP) is a powerful analytical tool that visualizes a molecule's size, shape, and the distribution of its electrostatic potential, which is color coded to indicate positive, negative, and neutral regions. It is instrumental in elucidating the relationship between molecular structure and physicochemical properties. The MESP map effectively highlights reactive sites: red areas typically denote electron rich (nucleophilic) zones, blue indicates electron deficient (electrophilic) regions, and green represents neutral potential. For the 2phap ligand and its metal complexes illustrated in Figure

6, the electron-rich red and yellow regions mark sites susceptible to electrophilic attack, whereas the electron-deficient blue region is prone to nucleophilic attack. The gradient of electrostatic potential is represented by the color scale: red < orange < yellow < green < blue [26]

3.6. Antimicrobial activities

The antimicrobial activities of synthesized compounds (2phap, 2phapCo, 2phapNi, and 2phapZn) were evaluated against *Staphylococcus aureus*, *Escherichia coli*, and *Candida albicans* at concentrations of 25–100 µg/mL are shown in Table 6. Notably, 2phapCo and 2phapZn exhibited superior antibacterial and antifungal activities, with inhibition zones reaching 24–27 mm, shown in Figure 7, thereby outperforming standard drugs Chloramphenicol and Fluconazole. While 2phapNi demonstrated moderate efficacy, the parent ligand 2phap showed the least activity. The enhanced antimicrobial effects observed for the metal complexes are attributed to improved membrane penetration and reactive oxygen species (ROS) generation. Overall, coordination with Co^{2+} and Zn^{2+} significantly boosted the antimicrobial potential of the tetra aza macrocyclic ligand, positioning 2phapCo and 2phapZn as promising dual action therapeutic candidates [27].

S. no.	Compound	Conc. µg / mL	Zone of inhibition (diameter in mm)		
			Antibacterial studies		Antifungal studies
			s. aureus	*E. Coli*	*C.albicans*
1	2phap	25	12	15	13
		50	16	17	17
		75	19	20	19
		100	22	22	23
2	2phapCo	25	17	19	20
		50	21	22	23
		75	22	23	25
		100	24	24	26
3	2phapNi	25	15	14	14
		50	19	19	20
		75	20	21	22
		100	23	23	23
4	2phapZn	25	13	13	15
		50	20	24	18
		75	22	25	19
		100	24	27	27
5.	Chloramphenicol	100	20	20	-
	Fluconazole	100	-	-	21

Table 6. The antimicrobial data of the 2phap ligand and its complexes

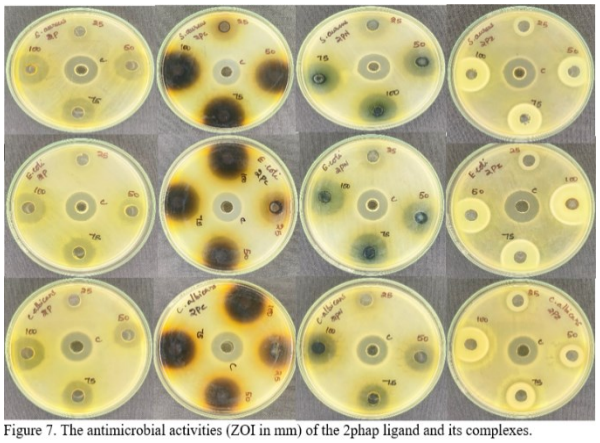

Figure 7. The antimicrobial activities (ZOI in mm) of the 2phap ligand and its complexes.

3.7. Antioxidant Activity

The antioxidant activity of the synthesized compounds (2phap, 2phapCo, 2phapNi, and 2phapZn) was concentration dependent over the 10–50 µg/mL range. Among these, 2phapZn exhibited the highest scavenging activity (55.66% at 50 µg/mL), followed in decreasing order of efficacy by 2phapNi (50.87%), 2phap (48.32%), and 2phapCo (42.10%). However, all synthesized compounds were less potent than the standard, Ascorbic Acid, which achieved 81.02% activity[28]. Thus, within the synthesized series, 2phapZn was identified as the most promising antioxidant as shown in Figure 8.

s.no.	Conc µg/ mL	2phap	2phapCo	2phapNi	2phapZn	Ascorbic acid (positive control)
1	10	21.8501	18.5008	23.1260	25.0398	55.8214
2	20	27.1132	21.0562	29.8246	33.3333	63.1579
3	30	34.7687	26.6348	36.2042	41.9458	69.5375
4	40	42.1053	35.4067	44.1736	49.9203	74.3222
5	50	48.3254	42.0526	50.8772	55.6619	81.0207

Table7.The antioxidant screening of the 2phap ligand and its complexes

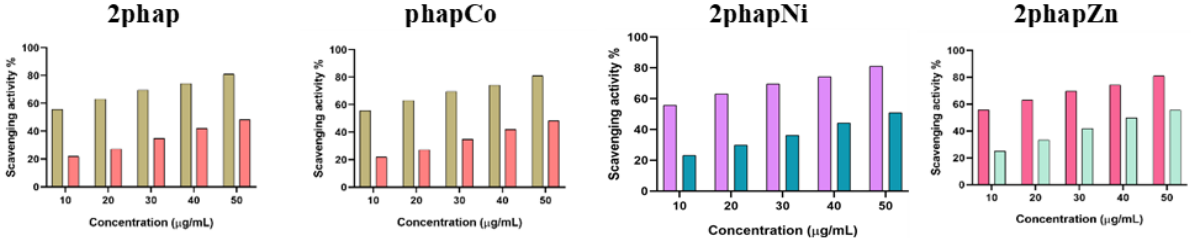

Figure 8. The graphical representation of antioxidant activity of the 2phap ligand and its metal complexes

3.8. in vitro cytotoxicity studies

The cytotoxic efficacy of the tetra-aza macrocyclic ligand 2phap and its transition metal complexes (2phapCo, 2phapNi, and 2phapZn) was evaluated against the U87 human glioblastoma cell line as depicted by Figure 9. All compounds exhibited significant, dose-dependent antiproliferative activity[29]. Notably, 2phapZn demonstrated the highest cytotoxicity (IC_{50} = 13.35 µg/mL), followed by 2phapNi (13.56 µg/mL), 2phapCo (14.10 µg/mL), and the free ligand 2phap (15.65 µg/mL) as shown in Table 8. These findings indicate that metal coordination, particularly with Zn(II), enhances the cytotoxic potential of 2phap against glioblastoma cells, highlighting 2phapZn as a promising candidate for further therapeutic development.

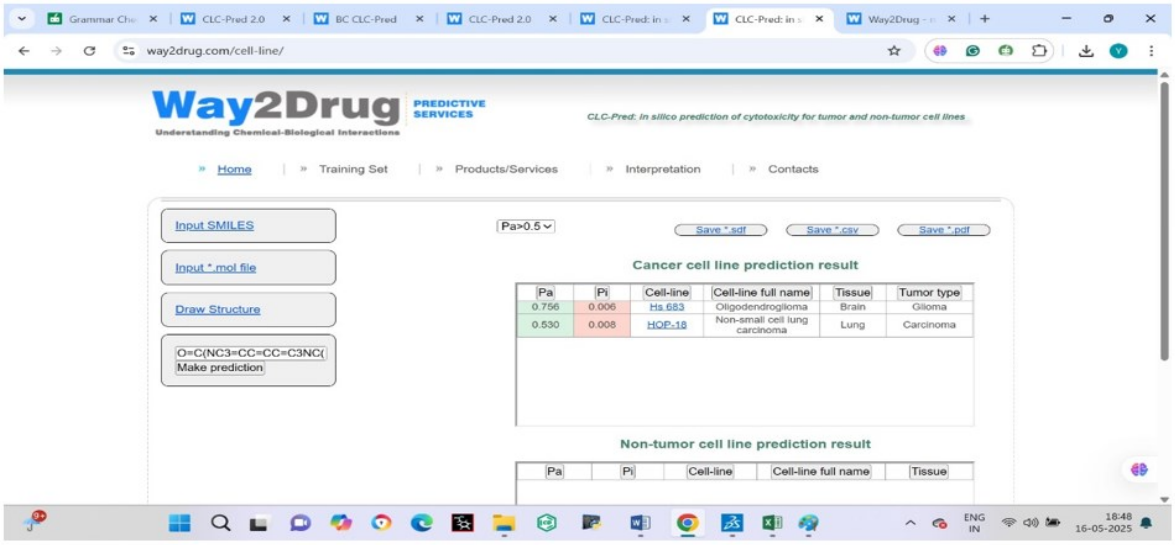

Figure 9. CLC-Pred: A web-service for prediction of human cell line cytotoxicity for drug-like compounds (for the 2phap ligand)

s.no.	Conc µg / mL	viability			
		2phap	2phapCo	2phapNi	2phapZn
1	0	100	100	100	100
2	10	74	66	65	63
3	20	37	36	33	36
4	30	17	15	15	10
5	40	8	5	5	2
6	50	0	0	0	0
7	IC_{50}	15.65	14.10	13.56	13.35

Table 8. The *Invitro* Cytotoxic activity of the 2phap ligand and its complexes towards the U87 human cancer cell line with IC_{50}

3.9. Apoptosis Dual Staining

The apoptotic activity of synthesized metal-doped 2phap compounds in U87 cells was confirmed by Acridine Orange/Ethidium Bromide (AO/EB) staining. At IC_{50} concentrations, 2phapZn notably induced substantial apoptosis, evidenced by a high proportion of red/orange (apoptotic/dead) to green (viable) fluorescent cells, surpassing other complexes and untreated controls (which remained viable)[30]. Morphological changes and increased red/orange fluorescence in complex-treated cells further confirmed apoptosis. These findings, consistent with MTT cytotoxicity data shown in Figure 10, highlights that Zn (II) coordination significantly enhances the pro-apoptotic potential of the ligand (Figure 2).

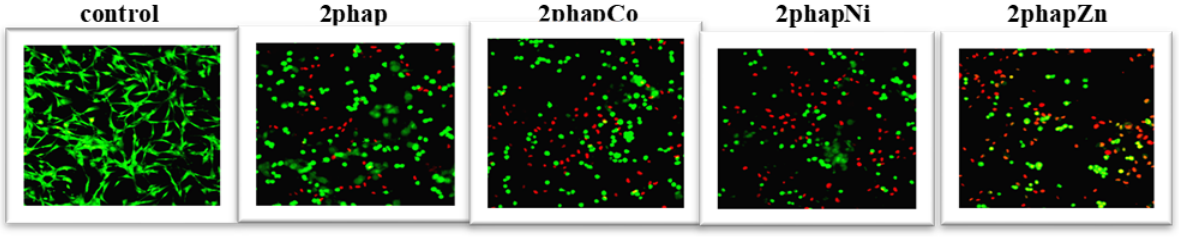

Figure 10 The pictorial representation of induced apoptosis in U87 human cell line by AO-EB staining method by the 2phap ligand and its complexes

CONCLUSION

The comprehensive evaluation of the zinc-based macrocyclic complex 2phapZn underscores its potential as a promising HDAC2 inhibitor with significant therapeutic relevance for brain glioma. Despite its deviation from Lipinski's rule of five, 2phapZn demonstrated superior binding affinity to HDAC2, evidenced by a docking score of –8.7 kcal/mol and strong interactions with key catalytic residues such as HIS183 and PHE155. The compound also exhibited the highest electrophilicity index and lowest HOMO–LUMO bandgap among its analogs, indicating pronounced electronic reactivity favorable for biological activity. Importantly, in vitro cytotoxicity studies revealed potent antiproliferative effects on U87 glioma cells, with an IC_{50} value of 13.38 µg/mL, surpassing both the parent ligand and other metal complexes. Combined with its favorable safety profile, non-carcinogenic nature, and moderate antioxidant and antimicrobial properties, 2phapZn emerges as a viable candidate for further development in HDAC-targeted glioma therapy, particularly via non-oral or localized delivery strategies

REFERENCES

- Subhash, Jyoti, Gupta, M., Phor, A., & Chaudhary, A. (2023). Synthesis, spectral characterisation, in vitro cytotoxicity, antimicrobial, antioxidant, DFT and molecular docking studies of Ru(III) complexes derived from amide-based macrocyclic ligands. Research on Chemical Intermediates, 50(3), 1081–1111.
- Chang, X., Fan, M., Gu, C.-F., He, W.-H., Meng, Q., Wan, L.-J., & Guo, Y.-G. (2022). Selective Extraction of Transition Metals from Spent LiNixCoyMn1−x−yO2 Cathode via Regulation of Coordination Environment. Angewandte Chemie, 61(24).
- Kumar, S., & Gupta, R. (2014). Endogenous and Exogenous Ligand-Dependent Formation of a Superoxide-Bridged Dicobalt(III) Complex and Mononuclear CoIII Complexes with Amide-Based Macrocyclic Ligands. European Journal of Inorganic Chemistry, 2014(32), 5567–5576.
- Vinod Kumar VASHISTHA, MITTAL, A., BALA, R., DAS, D. K., & SINGH, P. P. (2023). Synthesis, characterization, electrochemical and antibacterial studies of MN4-type macrocyclic complexes of Ni(II). Revue Roumaine de Chimie, 68(9), 447–452.
- Dong, J., Zhu, X., Yu, W., Hu, X., Zhang, Y., Yang, K., You, Z., Liu, Z., Qiao, X., & Song, Y. (2022). Pyrazolo [3,4-d]pyrimidine-based dual HDAC/Topo II inhibitors: Design, synthesis, and biological evaluation as potential antitumor agents. Journal of Molecular Structure, 1272, 134221–134221.
- Li, Y., & Seto, E. (2016). HDACs and HDAC Inhibitors in Cancer Development and Therapy. Cold Spring Harbor Perspectives in Medicine, 6(10), a026831.
- Etienne Bonvin, Hippolyte Personne, Thierry Paschoud, Reusser, J., Gan, B.-H., Luscher, A., Thilo Köhler, Delden, C. van, & Reymond, J.-L. (2023). Antimicrobial Peptide–Peptoid Hybrids with and without Membrane Disruption. ACS Infectious Diseases, 9(12), 2593–2606.
- Sirelkhatim, A., Mahmud, S., Seeni, A., Kaus, N. H. M., Ann, L. C., Bakhori, S. K. M., Hasan, H., & Mohamad, D. (2015). Review on Zinc Oxide Nanoparticles: Antibacterial Activity and Toxicity Mechanism. Nano-Micro Letters, 7(3), 219–242.
- Millan, M. J., Dekeyne, A., Gobert, A., Brocco, M., Mannoury la Cour, C., Ortuno, J.-C., Watson, D., & Fone, K. C. F. (2020). Dual-acting agents for improving cognition and real-world function in Alzheimer's disease: Focus on 5-HT6 and D3 receptors as hubs. Neuropharmacology, 177, 108099.
- Gülçin, İ., & Alwasel, S. (2023). DPPH radical scavenging assay. Processes, 11(8), 2248–2248, https://doi.org/10.3390/pr11082248
- Faubert, B., Solmonson, A., & DeBerardinis, R. J. (2020). Metabolic reprogramming and cancer progression. Science, 368(6487), eaaw5473.
- Kumar, N. N., lal, N. N., None Vishal Nemaysh, & Mehta, P. (2023). Synthesis and in vitro anticancer activity of novel 1,4-dimethyl-9-H-carbazol-3-yl) methanamine derivatives against human glioma U87 MG cell line. World Journal of Advanced Research and Reviews, 19(1), 1099–1108.
- Eriksson, I., Vainikka, L., Persson, H. L., & Öllinger, K. (2023). Real-Time Monitoring of Lysosomal Membrane Permeabilization Using Acridine Orange. Methods and Protocols, 6(4), 72.
- Daina, A., Michielin, O., & Zoete, V. (2017). SwissADME: a Free Web Tool to Evaluate pharmacokinetics, drug-likeness and Medicinal Chemistry Friendliness of Small Molecules. Scientific Reports, 7(1), 1–13.
- A. Ibrahim, A., Ibrahim, M. A., Sulliman, E. A., Daood, S. M., & Ismael, G. Q. (2021). Comparison Study of HOMO-LUMO Energy Gaps for Tautomerism of Triazoles in Different Solvents Using Theoretical Calculations. NTU Journal of Pure Sciences, 1(1), 38–43.
- Oller, J., & Jaque, P. (2023). Connection between nuclear and electronic Fukui functions beyond frontier molecular orbitals. The Journal of Chemical Physics, 159(12).
- Anant Babu Marahatta. (2020). DFT Study on Electronic Charge Distribution and Quantum−Chemical Descriptors for the Kinetic Stability of Vanadium Aquo Complex Ions [V(H2O)6]2+ and [V(H2O)6]3+. International Journal of Progressive Sciences and Technologies, 22(1), 67–81.
- Thommes, M. (2016). Physisorption of gases, with special reference to the evaluation of surface area and pore size distribution (IUPAC Technical Report). Chemistry International, 38(1), 25–25.
- Corso, G., Hannes Stärk, Jing, B., Barzilay, R., & Jaakkola, T. S. (2022). DiffDock: Diffusion Steps, Twists, and Turns for Molecular Docking.
- Khandar, A. A., Kirschbaum, K., Abedi, M., Mock, K., Tracy, G., Spasojevic, V., & Hosseini-Yazdi, S. A. (2015). Synthesis, characterization and crystal structures of mono and dinuclear macrocyclic cobalt(ii) complexes with a new tetraaza m-xylyl-based macrocyclic ligand. New Journal of Chemistry, 39(4), 2822–2831.
- Aqra F MAM, Shah SA, Jamhour RMAQ, Siddiqi KS, Al-Jowder O, Al-Saleh F. Transition Metal Complexes of a New 12-Membered Tetraaza Macrocycle. Synthesis and Reactivity in Inorganic and Metal-Organic Chemistry. 1994; Nov;24(9):1599–1612.
- Ayipo Y, Osunniran W, Badeggi U, Saheed I, Jimoh A, Babamale H, et al. Synthesis, characterization and antibacterial study of Co(II) and Cu(II) complexes of mixed ligands of piperaquine and diclofenac.JOTCSA. 2021;8(2):633–50,
- Synthesis, structural characterization, thermal analysis, DFT, biocidal evaluation and molecular docking studies of amide-based Co(II) complexes Subhash1 Ashu Chaudhary1 · Mamta1 · Jyoti2,Chemical Papers (2023) 77:5059–5078
- Effect of Ligand Architecture on the Structure and Properties of Square-Planar Nickel(II) Complexes of Amide-Based Macrocycles,Savita Sharma,Shailesh Upreti,Rajeev Gupta, European Journal of Inorganic Chemistry (Wiley), Vol. 2007, Iss: 20, pp 3247,
- Macrocyclic ligands designed to impose tetrahedral coordination: [1-(3-dimethylaminopropyl)-1,5,9-triazacyclododecane], L1, [1{2-(pyrrolidin-1-yl)ethyl}-1,5,9-triazacyclododecane], L2, and their zinc(II) complexes,Nathaniel W. Alcock, Andrew C. Benniston, Peter Moore, Graham A. Pike and Simon C. Rawle,***J. Chem. Soc., Chem. Commun.***, 1991, 706-708,

- Zahra Akbari a,b,1, Claudio Stagno b,1, Nunzio Iraci b, Thomas Efferth c, Ejlal A. Omer c,Anna Piperno b, Morteza Montazerozohori a, Mehran Feizi-Dehnayebi d,*, Nicola Micale, Biological evaluation, DFT, MEP, HOMO-LUMO analysis and ensemble docking studies of Zn(II) complexes of bidentate and tetradentate Schiff base ligands as antileukemia agents, Journal of Molecular Structure 1301 (2024) 137400,
- Sandhu Q, Pervaiz M, Majid A, Younas U, Saeed Z, Ashraf A, et al. Review: Schiff base metal complexes as anti-inflammatory agents. Journal of Coordination Chemistry. 2023; May 19;76(9-10):1094–1118.
- Muhammad, Araby A, Walla Alelwani, Kattan SW, Mansouri OA, Rasib M, et al. Green-synthesized nanoparticles of the polyherbal extract attenuate the necrosis of pancreatic ß-cell in a streptozotocin- induced diabetic model. Heliyon. 2023; May 1;9(5):e16137–7,
- Kumar P, Nagarajan A, Uchil PD. Analysis of Cell Viability by the MTT Assay. Cold Spring Harbor Protocols [Internet].2018; Jun;2018(6):pdb.prot095505.
- Sathiya Kamatchi T, Mohamed Subarkhan MK, Ramesh R, Wang H, Małecki JG. Investigation into antiproliferative activity and apoptosis mechanism of new arene Ru(ii) carbazole-based hydrazone complexes. Dalton Transactions. 2020;49(32):11385– 11395.